Controlled Grafting Synthesis of Silica-Supported Boron for Oxidative Dehydrogenation Catalysis

† Department of Chemistry, University of Wisconsin – Madison, 1101 University Avenue,

Madison, Wisconsin 53706, United States

Department of Chemical and Biological Engineering, University of Wisconsin – Madison, 1415 Engineering Drive, Madison, Wisconsin 53706, United States

§ Department of Chemistry, Iowa State University, 2438 Pammel Drive, Ames, Iowa, 50011,
United States

US DOE Ames Laboratory, Ames, Iowa, 50011, United States

‡ These authors contributed equally to this work.

KEYWORDS: chemical grafting; solid-state NMR; oxidative dehydrogenation; boron-containing catalysts; supported catalysts

Abstract. We present the controlled grafting synthesis of pinacolborane on amorphous silica. ¹¹B solid state NMR and IR spectroscopies reveal that the precursor molecule anchors monopodally to the surface and can form hydrogen-bonding interactions with neighboring unreacted silanol groups. The extent of hydrogen bonding can be controlled by the silica pretreatment dehydration temperature. Thermal treatment of the grafted boron materials under vacuum generates clusters of oxidized/hydrolyzed boron regardless of boron weight loading, illustrating that boron is highly mobile on the silica surface at elevated temperatures. The materials exhibit propane oxidative dehydrogenation activity expected for silica-supported boron catalysts. Interestingly, the kinetic behavior of these supported catalysts deviates from that of previously reported bulk boron materials, prompting further studies into the reaction kinetics over these materials. The synthetic and catalytic insights gained here can inform future studies of improved synthesis routes and reaction kinetics.

1. Introduction

Boron-based materials are promising catalysts for the selective oxidative dehydrogenation (ODH) of light alkanes to olefins.¹⁻⁶ The production of light olefins is an important industrial reaction that currently requires high energy consumption.⁷ Improvements in catalysts that produce light olefins can result in large energy savings for the chemical industry.⁸ In the ODH of propane to propylene, boron-based materials, such as hexagonal boron nitride (hBN), metal borides, and elemental boron, show higher selectivity to propylene (e.g., 80% selectivity at 8% conversion) than the previous state-of-the-art supported vanadium oxide catalysts (e.g., 60% selectivity at 8% conversion for V/SiO₂).¹ Importantly, the main side-product of propane ODH over boron-based materials is ethylene, another important olefin, rather than CO and CO₂ that is seen for supported

metal oxides. The origin and mechanism of this exceptional behavior has been the subject of many recent studies.⁹⁻¹⁷

ODH over boron-based catalysts is proposed to proceed via a radical mechanism. 9-10, 14, 18 The product distribution is mainly determined by the gas phase radical chemistry, with selectivity being controlled by the O₂ partial pressure. 3, 14 The role of the surface is to initiate the reaction by forming radicals that propagate in the gas phase, leading to the exceptional selectivity. 10 A mixed boron oxide/hydroxide phase, B₂(OH)_{2x}O_{3-x} (x = 0-3), has been identified by 11B solid-state NMR spectroscopy, along with electron microscopy, X-ray photoelectron and soft x-ray absorption spectroscopy, as necessary for catalytic activity. 15-16, 19-21 This boron oxide/hydroxide layer is predicted by theory to be highly dynamic at elevated temperature under an oxidizing atmosphere. 22 Under such conditions, the oxidized boron layer can access many stoichiometries of boron and oxygen and can form several structures within a given stoichiometry. A recent combined catalysis and theory study identified a metastable, unsaturated {BB} unit as a potential active site whose reactivity can explain the peculiar kinetic behavior observed for B-based ODH catalysts. 10

The unsaturated {BB} metastable active site hypothesis means that *ex situ* characterization cannot directly observe active species due to their short lifetime. Instead, *ex situ* characterization of catalysts before and after reaction is utilized to understand what type of boron species supported on the surface of silica are required to generate ODH active sites. For example, boron isomorphously substituted into a zeolite framework via hydrothermal synthesis (B-MWW) gives rise to stable BO₃-type species, with the major species being isolated **B**(OSi)₃ in the zeolite framework.¹⁷ Notably, B-MWW is inactive for propane ODH and does not restructure under reaction conditions. When boron is post-synthetically immobilized on the B-MWW surface *via* incipient wetness impregnation, producing agglomerated boron oxide/hydroxide, the material

becomes active for propane ODH.¹⁷ These results indicate that isolated BO₃ species are not active and that boron agglomeration is likely necessary for active site formation. This conclusion is in line with the theory-predicted boron-rich metastable active site and has led us to investigate the extent of boron agglomeration necessary for catalytic activity. Therefore, molecular-level control over the boron speciation is essential to better understand the extent of boron agglomeration required for catalytic activity, thus facilitating the rational design and development of next-generation ODH catalysts.

In our group's previous work with silica-supported boron oxide (B/SiO₂), we synthesized a series of B/SiO₂ materials with different weight loadings of boron via incipient wetness impregnation (B/SiO₂-IWI) using a triisopropyl borate solution.¹⁹ The motivation behind this synthesis was to generate different surface coverages of boron oxide, thereby generating different species ranging from isolated to polymeric to nanoparticulate, as is commonly done with supported metal oxides.²³⁻²⁴ Instead, we found that boron speciation – and propylene selectivity – was independent of boron weight loading. While we could observe that the supported boron oxide/hydroxide layer restructured during catalysis *via* ¹¹B solid-state NMR spectroscopy, the distribution of species and their dynamics under reaction conditions for the series of B/SiO₂-IWI catalysts made assigning reactivity to any individual structure intangible.

Grafting chemistry is often employed in catalyst synthesis to control the density and speciation of (transition metal) active sites. Such studies, coupled with detailed catalytic and spectroscopic characterization, have led to mechanistic insights for a variety of reactions such as olefin polymerization and hydrogenolysis. ²⁵⁻²⁶ Grafted materials can also be used to investigate the formation of active species; insights from such studies often inform the rational synthesis of improved catalytic materials. ²⁷⁻²⁸ In this study, we describe the controlled grafting synthesis of a

boron precursor on amorphous silica. Each grafted material is thermally treated to remove the thermolytic precursor²⁹⁻³⁰ and evaluated as a propane ODH catalyst. The structures of the asgrafted, thermally treated, and catalytically tested materials were determined by solid-state NMR and IR spectroscopies.

2. Experimental Methods

2.1 Material Synthesis

Bpin/SiO₂ materials were synthesized via grafting chemistry. Silica powder (Aerosil 300 from Evonik, specific surface area ca. 300 m²g⁻¹) was dehydrated overnight at 200, 700, or 900 °C under vacuum (20 µbar) and stored in a N₂ glovebox (\leq 1 ppm O₂ and H₂O) to prevent rehydration. These support materials are denoted as SiO_{2(T)}, where T refers to the dehydration temperature.

Pinacolborane (HBpin, Millipore-Sigma, distilled once before use) was deposited in the gas phase onto 500 mg pretreated silica cooled to -196 °C (5 equiv. based on initial silanol content) at ca. 20 µbar static vacuum (process illustrated in Figure S1). The transfer period (ca. 20 min) was followed by a reaction period at room temperature (30 min) and a mild thermal post-treatment at 50 °C and 20 µbar dynamic vacuum (1 h) to remove unreacted precursor. The materials at this stage are called Bpin/SiO_{2(T)} and stored in a N₂ glovebox. Thermal treatment of the Bpin/SiO_{2(T)} materials was done at 20 µbar dynamic vacuum and 500 °C (5 °C min⁻¹) for 10 hours. The materials at this stage are denoted in the figures as Bpin/SiO_{2(T)}-500v and ST (T = 2, 7, or 9, referring to the initial support dehydration temperature) in the text.

N,N-Bis(trimethylsilyl)methylamine, or $(TMS)_2NMe$, (Millipore-Sigma, distilled twice before use) was used for the silylation of $SiO_{2(700)}$ (denoted as TMS- $SiO_{2(700)}$). The silylating agent was exposed to the dried silica under 20 µbar vacuum in the same way as HBpin (using 5 equiv based

on initial silanol content) and thermally post-treated at 250 °C. Afterward, HBpin was deposited onto the silylated material to obtain Bpin/TMS-SiO₂₍₇₀₀₎ (5 equiv based on initial silanol content).

2.2 Catalytic Testing

Bpin/SiO_{2(T)}-500v catalysts were compressed using a pellet press (Pike Technologies; pressure program: 5 tons of force for 90 s and 7 tons of force for 60 s) and sieved to collect particles of 300–600 μm diameter to limit any potential mass transfer effects. About 25–50 mg of Bpin/SiO_{2(T)}-500v was diluted in quartz chips in a 1:2 ratio and loaded into a quartz reactor tube (8 mm i.d.) and supported on a bed of quartz wool in the middle of the tube. Additional quartz wool was used to pack the inside of the quartz tube lightly past the catalyst bed to reduce dead volume. Flow rates of C₃H₈ (instrument grade, Matheson), O₂ (UHP, Airgas), and N₂ (UHP, Airgas) were controlled by using three mass flow controllers (Bronkhorst) and calibrated to each individual gas to allow total flow rates of 40–200 mL min⁻¹. The H₂O produced from the reaction was condensed using a thermoelectrically cooled condenser held at −5 °C. The dried reactor effluent was monitored by using an online μGC (Inficon micro GC fusion gas analyzer) equipped with three GC modules and three microthermal conductivity detectors (μTCD). O₂, N₂, CH₄, and CO were analyzed by using a Rt-molsieve 5A column, CO₂ was analyzed by using an Rt-U-bond column, and all hydrocarbons apart from CH₄ were analyzed using an Rt-alumina bond/Na₂SO₄ column.

In each catalytic test, the reactor was heated to the reaction temperature of 500 °C under O₂ and N₂ flow. The temperature was controlled by using a thermocouple inserted into the middle of the catalyst bed. After the temperature was stabilized, the C₃H₈ feed was introduced and GC measurements were begun. As there is an induction period before catalytic activity is stabilized, each catalyst was treated for 24 h under a feed of 6:3:11 C₃H₈:O₂:N₂ at 40 mL min⁻¹. After this treatment, the gas flow rate was adjusted to give WHSV⁻¹ values ranging from 0.6 to 6.3 kg_{cat} s

 mol_{C3H8}^{-1} (ca. 40–200 mL min⁻¹), and further GC measurements were performed. Reported experiments showed the carbon balance closed within $\pm 3\%$.

2.3 Materials Characterization

IR Spectroscopy. IR spectra were recorded on a self-supporting wafer using a Bruker Alpha spectrometer in transmission mode (resolution of 2 cm⁻¹). Intensities were normalized to the Si–O–Si overtones of the silica framework. Analysis was performed inside a glovebox (<1 ppm of H₂O and O₂).

ICP-MS. Boron elemental analysis was performed with ICP-MS (Agilent 5110 ICP-MS). Prior to measurement, ~20 mg of sample was digested using 200 uL of 48 wt% HF (Sigma-Aldrich), after which the solution was diluted to 10 mL with DI water and diluted again to a 1:10 ratio for analysis. HF is extremely dangerous and should be handled with caution.

NMR Spectroscopy (UW Madison). One-dimensional direct excitation ¹¹B spin echo (Bpin/SiO_{2(T)}-500v materials) and dipolar double-quantum-single-quantum homonuclear correlation (Bpin/SiO_{2(T)}-500v materials) spectra were recorded at the University of Wisconsin – Madison on a 11.7 T ($v_0(^1H)$) = 500 MHz) Bruker standard bore NMR spectrometer equipped with an Avance III console and a 4 mm magic-angle spinning (MAS) HXY NMR probe. All samples were packed into 4 mm zirconia NMR rotors in an N₂ filled glovebox and spun with N₂ gas to avoid any hydration of the silica surface. Chemical shifts were calibrated on each sample with ¹H chemical shifts referenced to neat tetramethylsilane (TMS) with adamantane as a secondary chemical shift reference ($\delta(^1H)$) = 1.82 ppm). ¹¹B shifts were referenced using previously reported IUPAC recommended relative NMR frequencies. ³¹ All spectra were processed using the Bruker Topspin 3.6.1 NMR software.

Analytical simulations of the ¹¹B NMR spectra were performed using the solid lineshape analysis (sola) module implemented in Bruker Topspin 3.6.1.

All experimental details (magnetic field strength, number of scans, recycle delay, t_1 TD points, t_1 dwell (Δt_1), dipolar recoupling duration and total experimental times) are given in Table S1. 1D direct excitation ¹¹B NMR spectra were recorded with a rotor synchronized spin echo NMR pulse sequence. ¹¹B CT-selective $\pi/2$ and π pulse lengths were 8.2 and 16.4 μ s in duration, corresponding to a *ca.* 15.2 kHz RF field and *ca.* 30.4 kHz central-transition (CT) nutation frequency. ¹¹B dipolar DQ-SQ homonuclear correlation NMR experiments were recorded with the $R2_2^1$ homonuclear dipolar recoupling sequence. ³²⁻³³ A CT selective π pulse was applied during t_1 evolution to ensure only correlations from two ¹¹B spins are observed. ³²⁻³³ Rotor-assisted population transfer (RAPT) was applied \pm 500 kHz off resonance to the ¹¹B spins prior to all DQ-SQ NMR experiment to enhance the ¹¹B CT population. ³⁴⁻³⁶

NMR Spectroscopy (Iowa State University). Solid-state NMR spectra were recorded at $B_0 = 14.1$ T ($v_0(^1\text{H}) = 600$ MHz) or 9.4 T ($v_0(^1\text{H}) = 400$ MHz). The 14.1 T Bruker wide-bore NMR spectrometer was equipped with a Bruker Avance II console and a 2.5 mm magic angle spinning (MAS) HXY NMR probe configured in double resonance mode. The 9.4 T Bruker wide-bore NMR spectrometer was equipped with a Bruker Avance III HD console, a 3.2 mm MAS HXY dynamic nuclear polarization (DNP) NMR probe configured in double resonance mode and a Bruker DNP liquid N_2 cooled low temperature MAS unit to reach sample temperatures of ca. 100 K. All samples were packed into the appropriate size NMR rotor (zirconia 2.5 mm rotor or sapphire 3.2 mm rotor with a silicon plug) in an N_2 filled glovebox and spun with N_2 gas to avoid hydration. Chemical shifts were calibrated by using neat tetramethylsilane (TMS) with adamantane as a

secondary chemical shift reference ($\delta(^1H) = 1.82$ ppm). The 9.4 T chemical shifts were calibrated at 100 K by using the 1H NMR signal of frozen 1,1,2,2-tetrachloroethane (TCE) as a secondary chemical shift reference ($\delta(^1H) = 6.2$ ppm). ^{11}B and ^{29}Si shifts were referenced using previously reported IUPAC recommended relative NMR frequencies. 31 All spectra were processed using the Bruker Topspin 3.6.1 NMR software. Analytical simulations of the ^{11}B NMR spectra were performed using the solid lineshape analysis (sola) module as implemented in Bruker Topspin 3.6.1.

All experimental details (magnetic field strength, MAS frequency, number of scans, recycle delay, t_1 TD points, t_1 dwell (Δt_1), dipolar recoupling duration and total experimental times) are given in Table S1. A 1D ¹¹B rotor synchronized spin echo spectrum was recorded at $B_0 = 9.4$ T with 10 kHz MAS and a sample temperature of ca. 100 K. The ¹¹B central-transition (CT) selective $\pi/2$ and π pulse lengths were 10 and 20 μ s in duration, corresponding to a 12.5 kHz radio frequency (RF) field and 25 kHz CT nutation frequency. 100 kHz ¹H RF field of SPINAL-64 heteronuclear decoupling was performed throughout the entire spin echo sequence and acquisition of ¹¹B.³⁷

All solid-state NMR experimental details discussed below are with respect to spectra recorded on the 14.1 T NMR spectrometer. 1 H $\pi/2$ and π pulse lengths were 2.5 and 5.0 μ s in duration, corresponding to a 100 kHz RF field. 11 B CT-selective $\pi/2$ and π pulse lengths were 15 and 30 μ s in duration, corresponding to an 8.3 kHz RF field and 16.7 kHz CT nutation frequency. 1 H dipolar double-quantum-single-quantum (DQ-SQ) homonuclear correlation NMR experiments were recorded with the previously described back-to-back (BABA) NMR pulse sequence. $^{38-39}$ The $\pi/2$ pulse length in the homonuclear recoupling block was 2.5 μ s in duration, corresponding to a 100 kHz RF field. Each homonuclear recoupling block was 40 μ s in duration (1 rotor cycle). 1 H- 11 B

heteronuclear correlation (HETCOR) NMR experiments were performed with either (Bpin/SiO₂₍₂₀₀₎, all of the fresh and spent Bpin/SiO_{2(T)}-500v catalysts) ${}^{11}B \rightarrow {}^{1}H$ dipolar refocused INEPT (D-RINEPT) $^{40-41}$ or (Bpin/SiO₂₍₇₀₀₎ and Bpin/SiO₂₍₉₀₀₎) 1 H- 11 B t_1 -noise eliminated dipolar HMQC-3 (TONE DHMQC-3)⁴² NMR pulse sequences. 1D ¹¹B→¹H D-RINEPT and ¹H{¹¹B} TONE D-HMQC-3 experiments were performed on all samples to identify which experiment was more sensitivity (i.e., yielded largest signal intensity per unit of time). The pulse sequence with the greatest sensitivity was chosen to record 2D HETCOR spectra. All ¹H-¹¹B HETCOR NMR experiments were recorded with the symmetry-based $SR4_1^2$ heteronuclear dipolar recoupling sequence applied to the ¹H spins to re-introduce ¹H-¹¹B dipolar couplings (50 kHz RF field at 25 kHz MAS). 43 Rotor-assisted population transfer (RAPT) was applied \pm 550 or 650 kHz off resonance to the ¹¹B spins prior to all D-RINEPT experiments and during ¹H dipolar recoupling in TONE DHMQC-3 experiments to enhance the ¹¹B CT population. ³⁴⁻³⁶ ¹H { ¹¹B } TONE DHMQC-3 experiments were acquired with a 360 (9 rotor periods) or 480 (12 rotor periods) us 100 kHz ¹H RF field Lee-Goldberg (LG) spin-lock pulse (offset: 70.7 kHz – effective RF field: 122.4 kHz) to remove uncorrelated ¹H magnetization. ⁴² ¹H-detected ¹H-²⁹Si cross-polarization (CP) HETCOR experiments were performed with previously published NMR pulse sequences: ¹H→²⁹Si forward CP, ²⁹Si Z-filter, ¹H saturation at the HORROR condition (~ 400 ms in duration: 12.5 kHz RF field @ 25 kHz MAS) and ²⁹Si→¹H back CP for ¹H-detection. ⁴⁴⁻⁴⁵ Forward and backward ¹H→²⁹Si CP was achieved with simultaneous spin-lock pulses applied to the ¹H (with a 90-100 % ramp) and ²⁹Si spins with RF fields of *ca*. 60 and 32 kHz, respectively (25 kHz MAS). A schematic illustration of all pulse sequences is shown in Figure S2.

3. Results and Discussion

3.1 The effect of support dehydration temperature on HBpin grafting.

The controlled dispersion of boron on silica has mainly been studied for the synthesis of doped electronic materials. 46-47 The boron molecules used in these prior grafting studies react with the surface via organoboron or borane functionalities to generate single sites (structures shown in Figure S3). However, these compounds often require synthesis or have a long lead times from commercial sources. Here, we use pinacolborane (HBpin) to controllably graft boron onto the surface of silica. The choice of HBpin for grafting is based on the phenanthrene dioxoborane precursor used by Mathey *et al.* (Figure S3A), which appeared to generate controlled boron sites when grafted to SiO₂ dehydrated at 500 °C. 46 The B-H bond of HBpin can readily react with silanol groups and the steric bulk of the pinacol ring should prevent close spacing of anchored precursors and the self-reaction between two precursor molecules. Additionally, HBpin is commercially available and relatively inexpensive because of its abundant use in organic reactions.

Prior to grafting, amorphous SiO₂ was first dehydrated at different temperatures to control the silanol density, denoted as SiO_{2(T)}, where T = 200, 700, or 900 °C. All materials were handled in a N₂-atmosphere glovebox to minimize rehydration of the treated silica surface. HBpin was transferred in the gas phase under reduced pressures (20 µbar) into a cooled Schlenk flask containing the pretreated SiO_{2(T)}. When the transfer was complete, the flask was slowly warmed to room temperature and the contents lightly shaken to ensure uniformity of the sample. After a reaction period of 30 minutes, the material was post-treated at 50 °C under reduced pressure (20 µbar) to remove any unreacted precursor. The reaction between HBpin and isolated silanol groups is shown at the top of Figure 1. The material at this stage is called Bpin/SiO_{2(T)}.

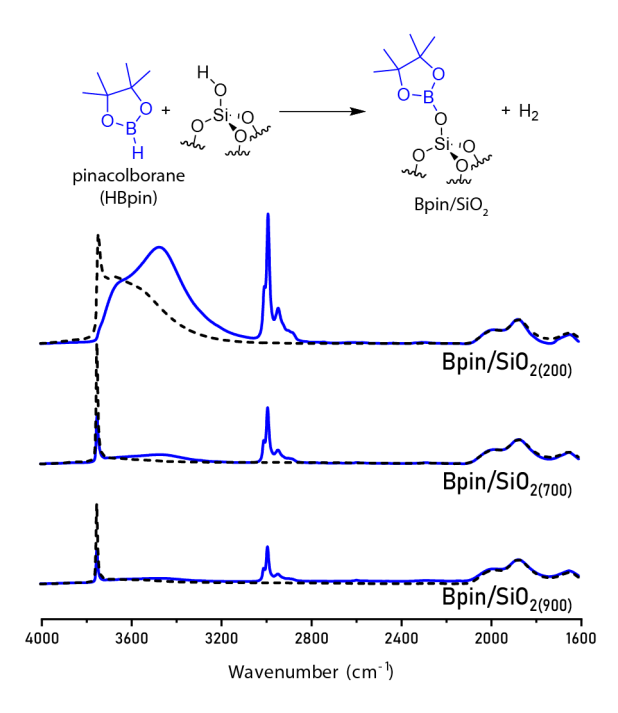


Figure 1. Transmission IR spectra of SiO₂ supports (black dashed lines) and HBpin grafted materials (blue solid lines). The intensity of each spectrum is normalized to the Si-O-Si overtone features at ca. 1870 cm⁻¹.

The structure of the grafted Bpin/SiO_{2(T)} materials was probed by Fourier Transform Infrared (FTIR) and solid-state NMR spectroscopies. Transmission FTIR spectra of SiO_{2(200,700,900)} contain a sharp peak at 3747 cm⁻¹ which can be assigned to isolated silanol groups (Si-OH, Figure 1 – black dashed lines). ⁴⁸⁻⁴⁹ SiO₂₍₂₀₀₎ features an intense, broad peak extending to *ca.* 3200 cm⁻¹ which corresponds to hydrogen-bonded silanol groups. Not surprisingly, this broad feature extending from *ca.* 3750 – 3200 cm⁻¹ is absent for the SiO_{2(700,900)} materials, consistent with reduced silanol density caused by increased dehydration temperatures (Table S2). After grafting with HBpin, new features in the C-H stretching region (3000-2850 cm⁻¹) appear, corresponding to the methyl groups of the Bpin precursor (Figure 1 – blue solid lines). There is an accompanying decrease in the signal intensity for isolated silanol groups at 3747 cm⁻¹. For Bpin/SiO₂₍₂₀₀₎, nearly 100% of the isolated silanol groups are consumed while only *ca.* 70% of isolated silanols on SiO₂₍₇₀₀₎ and SiO₂₍₇₀₀₎ react

with the precursor. Additionally, on each Bpin/SiO $_{2(T)}$ sample, a new, broad signal in the OH region appears, indicating a new hydrogen-bonding interaction upon grafting. This new hydrogen-bonding interaction is likely between an unreacted Si-OH group and grafted Bpin molecule. As expected, the intensity of the hydrogen-bonding feature is significantly reduced with increasing SiO $_2$ thermal treatment temperatures.

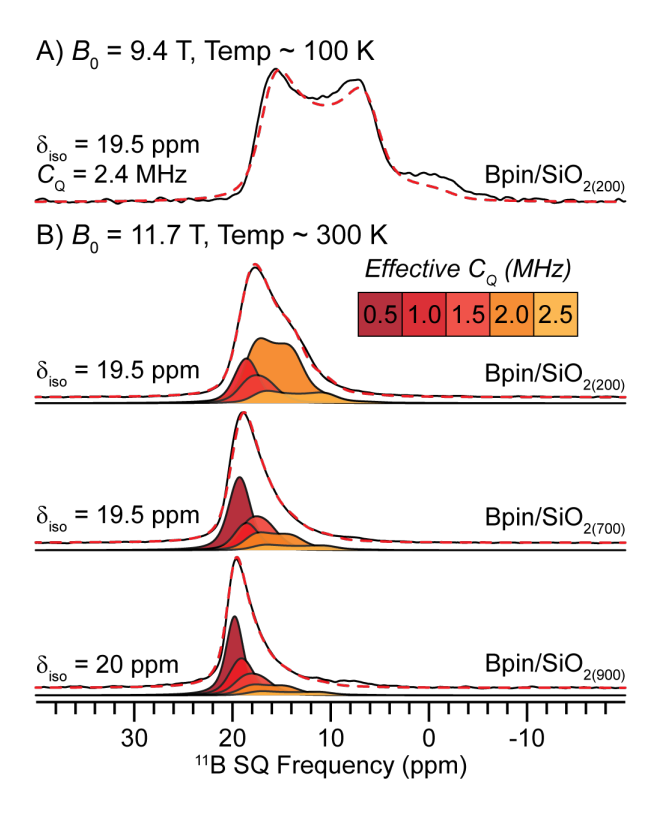
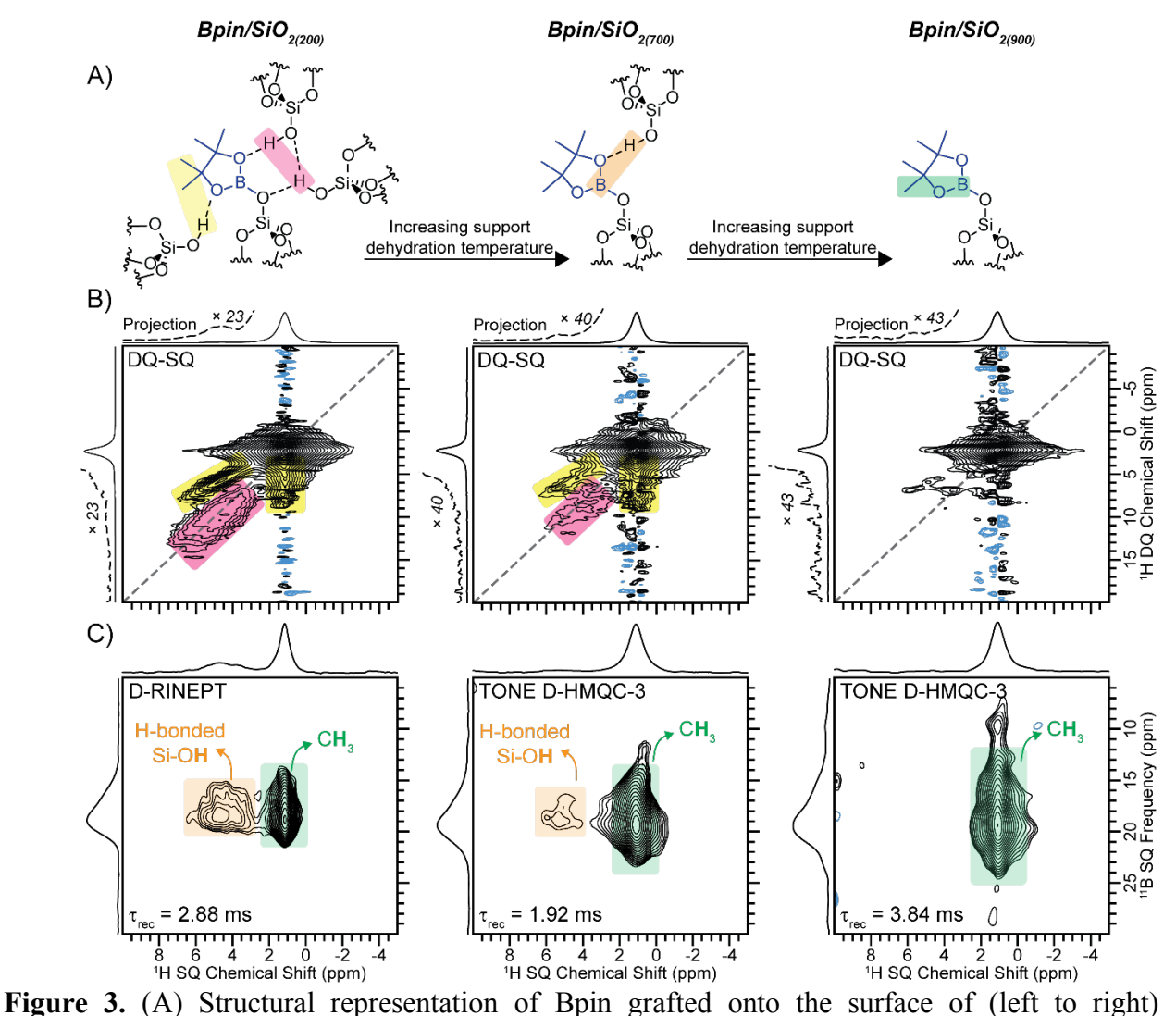


Figure 2. 1D direct excitation ¹¹B NMR spectra of (A and B, upper) Bpin/SiO₂₍₂₀₀₎, (B, middle) Bpin/SiO₂₍₇₀₀₎ and (B, lower) Bpin/SiO₂₍₉₀₀₎ recorded at (A) 100 K and $B_0 = 9.4$ T with 10 kHz MAS or (B) room temperature and $B_0 = 11.7$ T with either (upper, lower) 10 or (middle) 12 kHz MAS. (A) The ¹¹B NMR spectrum was analytically simulated to a single site (red dashed line): $\delta_{iso} = 19.5$ ppm, $C_Q = 2.4$ MHz and $\eta = 0$. (B) The ¹¹B NMR spectra were fit to multiple sites with identical δ_{iso} but varying C_Q from 0.5 - 2.5 MHz to represent partial averaging of the EFG tensor via reorientation about the B-O-Si bond (see Figure 1).

Solid-state NMR spectroscopy was used to further characterize the grafting of HBpin onto the SiO_{2(T)} surface and probe the local hydrogen-bonding network surrounding the grafted Bpin molecule. One-dimensional (1D) direct excitation ¹¹B NMR spectra of Bpin/SiO₂₍₂₀₀₎ were recorded at a sample temperature of either ca. 100 K or room temperature (Figure 2A, 2B upper, respectively). Interestingly, the two ¹¹B NMR spectra display significantly different features. At 100 K, a single, well-defined central-transition (CT) ¹¹B quadrupolar powder pattern is observed and can be simulated with an ¹¹B isotropic chemical shift (δ_{iso}) of 19.5 ppm, a quadrupolar coupling constant (C_0) of 2.4 MHz and a quadrupolar asymmetry parameter (η) of 0, typical of 3-coordinate BO₃ species. 15, 21, 50-53 However, at room temperature, the lower frequency horn of the quadrupolar powder pattern is mostly absent, and the center of gravity peak position is shifted to a higher frequency (Figure 2B, upper). The observation of a narrower signal with a higher center of gravity peak position at room temperature versus 100 K suggests that the ¹¹B electric field gradient (EFG) tensors are being partially averaged due to molecular motion. The partial averaging of the EFG tensors will essentially lead to a smaller effective C_0 . 54-55 Indeed, the room temperature ¹¹B NMR spectrum can be analytically simulated to multiple sites with $\delta_{iso}(^{11}B)$ of 19.5 ppm and C_0 varying from 0.5 to 2.5 MHz. Thus, comparison of room and low temperature ¹¹B NMR spectra reveal that Bpin/SiO₂₍₂₀₀₎ contains only one boron species: Bpin monopodally grafted onto the silica surface (Figure 1 – upper). The distribution in C_0 observed for the room temperature ¹¹B NMR spectrum illustrates a distribution in the degree of mobility (i.e., monopodal rotation about the B-O-Si bond). 1D ¹¹B NMR spectra of Bpin/SiO_{2(700, 900)} were also recorded at room temperature and display similar trends observed for Bpin/SiO₂₍₂₀₀₎, confirming the presence of only monopodally grafted Bpin (Figure 2B, middle and lower). Interestingly, the 1D ¹¹B NMR spectra become narrower with increasing support thermal treatment temperature, indicating that a higher fraction of surface boron

species undergo faster reorientation. The difference in the degree of rotation is likely due to a reduced number of hydrogen-bonding silanol species surrounding the grafted Bpin molecule, consistent with the IR spectra discussed above. It should be noted that the room temperature ¹¹B NMR spectra of Bpin/SiO_{2(T)} are consistent with that previously reported by Eedugurala *et al.*⁵⁶ Below, two-dimensional (2D) ¹H dipolar double-quantum-single-quantum (DQ-SQ) homonuclear and ¹H-¹¹B heteronuclear correlation (HETCOR) spectra of Bpin/SiO_{2(200, 700, 900)} confirm molecular structure and further probe the hydrogen bonding network surrounding the grafted Bpin molecule. Figure 3A illustrates the proposed structures supported by the spectra in Figures 3B and C.



Bpin/SiO₂₍₂₀₀₀₎, Bpin/SiO₂₍₇₀₀₀₎ or Bpin/SiO₂₍₉₀₀₀₎. The number of near-by silanol groups is not exact and is merely used to illustrate the correlations observed in the 2D (B) 1 H DQ-SQ and (C) 1 H- 11 B HETCOR spectra. The highlight boxes on the structures match the highlighted correlations overlaid on the 2D spectra. 1 H- 11 B HETCOR spectra were recorded using either [Bpin/SiO₂₍₂₀₀₀₎] 11 B \rightarrow 1 H D-RINEPT⁴⁰⁻⁴¹ or [Bpin/SiO_{2(7000, 9000)}] 11 H{ 11 B} TONE D-HMQC-3⁴² pulse sequences. All NMR spectra were recorded at room temperature and $B_0 = 14.1$ T with 25 kHz MAS.

A 2D ¹H dipolar DQ-SQ homonuclear correlation NMR spectrum of Bpin/SiO₂₍₂₀₀₎ reveals intense autocorrelations for ¹H SQ NMR signals ca. 1.5 and 4 - 7 ppm, corresponding, respectively, to the CH₃ methyl signals of Bpin and hydrogen-bonded silanol species on the silica surface (Si-OH - - HO-Si, Figure 3B, left and S4).⁵⁷ In addition, strong off-diagonal correlations are observed between the CH₃ methyl signals of Bpin and the hydrogen bonded silanol species (CH₃ - - HO-Si, Figure 3B, left). The observed off-diagonal correlations reveal that silanol species are in close spatial proximity to the grafted Bpin molecule and the autocorrelations at ca. 4-7ppm confirm that there are multiple silanol species surrounding the Bpin molecule in a hydrogenbonded nest. A 2D ¹H-¹¹B HETCOR spectrum of Bpin/SiO₂₍₂₀₀₎ further confirms that the silanol species are in close spatial proximity to the grafted Bpin molecule (Figure 3C, left), leading to the molecular structure proposed in Figure 3A (left). Here, three neighboring silanol groups are proposed to be surrounding the Bpin molecule based on integration of a ¹H direct excitation NMR spectrum (Figure S5). However, it should be noted that there is likely a significant source of error in this integration due to extensive signal broadening and the possibility of other types of hydrogen bonded silanols occurring on the surface. Nevertheless, the 2D spectra confirm that there are multiple silanol groups surrounding the grafted Bpin molecule in a hydrogen-bonded nest (Figure 3A, left).

2D ¹H DQ-SQ NMR spectra of Bpin/SiO_{2(700,900)} both display strong autocorrelations for ¹H SQ NMR signals at *ca.* 1.5 ppm which correspond to the CH₃ methyl signals of Bpin (Figure 3B, middle, right). Interestingly, the intensity of the H-bonded silanol autocorrelations (colored pink) and methyl to silanol off-diagonal correlations (colored yellow) are significantly reduced for Bpin/SiO₂₍₇₀₀₎ as compared to Bpin/SiO₂₍₂₀₀₎ and are near absent in Bpin/SiO₂₍₉₀₀₎ (Figure 3B), suggesting a reduced number of neighboring silanol species to the grafted Bpin molecule.

Comparison of 2D ¹H-¹¹B HETCOR spectra of Bpin/SiO_{2(200, 700, 900)} show identical trends observed in the 2D ¹H DQ-SQ spectra, where Bpin/SiO₂₍₇₀₀₎ displays significantly reduced correlations between nearby silanol species and the grafted Bpin molecule whereas these correlations are absent for Bpin/SiO₂₍₉₀₀₎ (Figure 3C, orange color). The observed reduction in the number of hydrogen bonded silanol species to the grafted Bpin molecule is consistent with the room temperature ¹¹B NMR and transmission IR spectra discussed above. Therefore, we illustrate that Bpin/SiO₂₍₂₀₀₎ contains multiple silanol species in a hydrogen-bonded nest surrounding the monopodally grafted Bpin molecule, while the number of nearby silanol species is significantly reduced for Bpin/SiO₂₍₇₀₀₎ and are near absent for Bpin/SiO₂₍₉₀₀₎, meaning Bpin is relatively isolated on the silica surface (Figure 3A).

To summarize, pinacolborane (HBpin) grafted in the gas phase onto silica results in selective monopodal anchoring of Bpin to the surface by reaction with an Si-OH group (Figure 1, upper). Neighboring unreacted Si-OH groups can form hydrogen-bonding interactions with the grafted molecule, limiting the degree of rotation of Bpin around the B-O-Si bond. The hydrogen-bonding environment around the grafted Bpin molecule depends on the density of surface silanol groups, which can be controlled by the support dehydration temperature (Figure 3A).

3.2 Formation of active ODH catalysts.

The grafted Bpin/SiO_{2(T)} materials were thermally treated at 20 µbar and 500 °C for 10 hours to remove the organics and generate the active catalysts. The materials after thermal treatment are denoted in the Figures as Bpin/SiO_{2(T)}-500v. As a shorthand in the text, the materials will be referred to as **S2**, **S7**, and **S9**, where the number corresponds to the initial support dehydration temperature (*i.e.*, **S2** corresponds to an initial support dehydration temperature of 200 °C). The boron weight

loadings (determined via ICP-MS) and BET surface areas are 1.65 ± 0.01 % and 246 m²g⁻¹, 0.81 ± 0.01 % and 271 m²g⁻¹, and 0.18 ± 0.01 % and 252 m²g⁻¹ for **S2**, **S7**, and **S9**, respectively (Table S2).

Transmission IR spectra of the thermally treated materials do not show aliphatic C-H stretching near 3000 cm⁻¹, indicating complete removal of the Bpin methyl groups (Figure S6). The IR spectra display two sharp features at 3747 and 3704 cm⁻¹, corresponding to SiO-H and BO-H stretching, respectively.^{21, 49, 58-59} In addition, all materials show a broad peak extending to *ca.* 3200 cm⁻¹ that can be assigned to hydrogen bonded SiO-H and/or BO-H species. As expected, the intensity of this broad hydrogen bonded hydroxyl signal is reduced with increasing silica thermal treatment temperatures.

We note that the experimentally determined boron weight loadings on S2 and S7 are higher than that calculated based on the initial silanol content, assuming HBpin grafts exclusively to isolated silanol species (Table S2). SiO₂ dehydrated at 700 °C has a silanol density of ca. 0.9/nm².⁴⁹ The stoichiometric reaction of HBpin with isolated SiOH groups would result in a boron weight loading of 0.48 wt %. The discrepancy between the calculated (0.48 wt %) and measured (0.81 wt %) boron loadings can be explained by the reaction of HBpin with the strained siloxane bridges that form at high dehydration temperatures. The reaction between strained siloxane bridges and a precursor has been previously observed when grafting vanadium triisopropoxide to SiO₂₍₇₀₀₎.²⁸ Indeed, when the silanol groups on SiO₂₍₇₀₀₎ are capped with trimethylsilane (TMS) groups (TMS-SiO₂₍₇₀₀₎), leaving only siloxane bridges as possible anchoring sites (Table S2), HBpin can anchor to the surface as seen by IR spectroscopy (Figure S7), resulting in a boron weight loading of 0.56 \pm 0.01 % (Table S2). Silica dehydrated at 200 °C has an isolated SiOH density of 1.2/nm² and the surface is additionally populated by hydrogen-bonding silanol nests.⁴⁹ Silanol nests are often

assumed to be relatively unreactive; however, a recent study of the grafting synthesis of vanadium triisopropoxide on SiO₂₍₂₀₀₎ revealed that the presence of a hydrogen-bond acceptor on the surface can activate H-bonding silanols as additional anchoring sites.²⁷ Given the formation of new H-bonding interactions upon the grafting of HBpin onto SiO₂₍₂₀₀₎, we propose that a similar activation of H-bonding silanols occurs, increasing the boron content of the sample. Unlike the **S2** and **S7** materials, the **S9** sample does not show a discrepancy between expected and measured boron loadings (Table S2). The agreement between calculated and measured weight loadings on **S9** indicates a change in reactivity of siloxane bridges on the SiO₂₍₉₀₀₎ support. This change in reactivity is likely associated with the partial collapse of the SiO₂ framework that occurs above 800 °C, which is supported by a decreased BET surface area determined for **S9** compared to **S7** (Table S2).⁴⁹

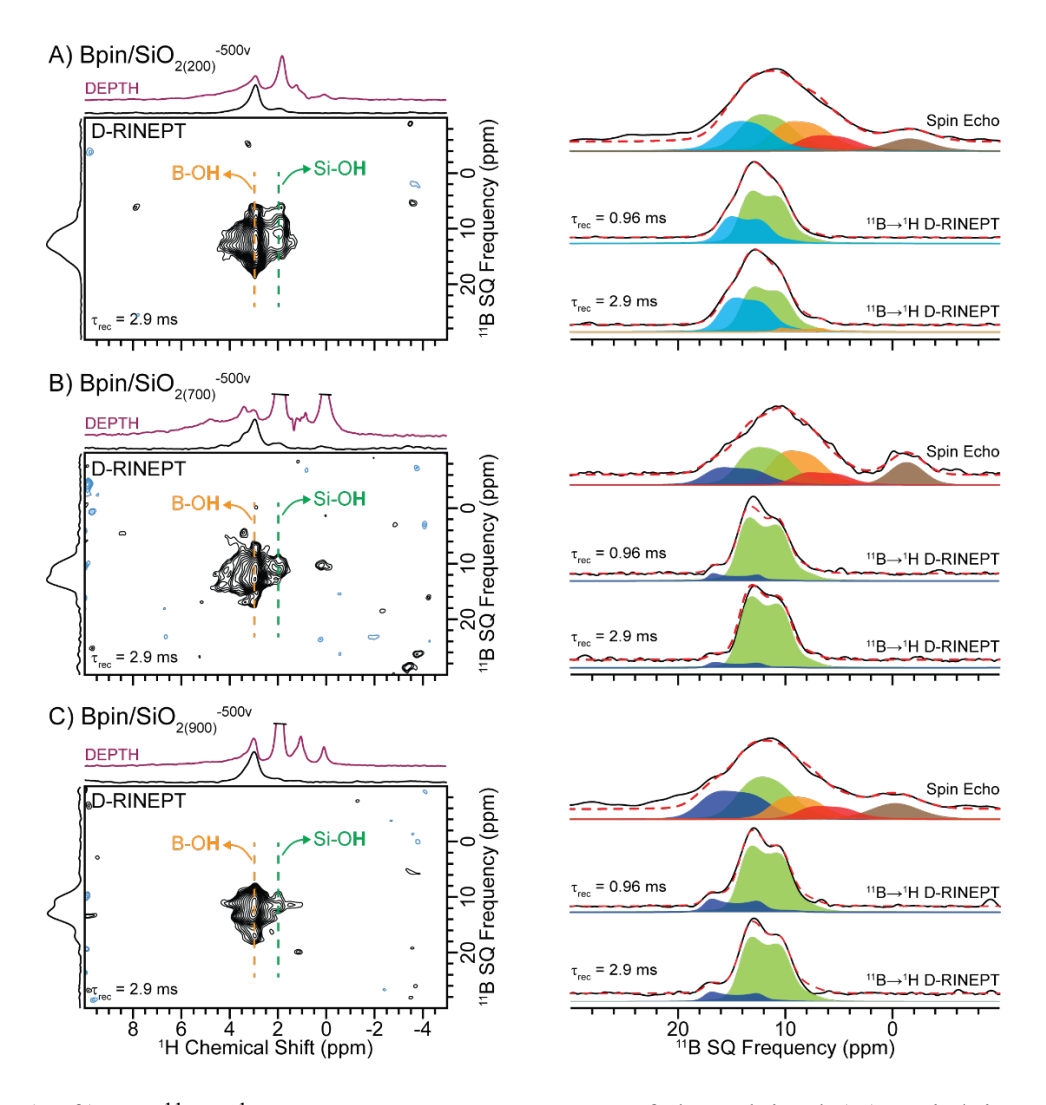


Figure 4. (Left) 2D ¹¹B→¹H D-RINEPT NMR spectra of the calcined (A) Bpin/SiO₂₍₂₀₀₎, (B) Bpin/SiO₂₍₇₀₀₎ and (C) Bpin/SiO₂₍₉₀₀₎ fresh catalysts. (Right) Comparison of (recycle delay ≥ 5 × T_1) 1D ¹¹B spin echo NMR spectra with ¹¹B projections from the 2D ¹¹B→¹H D-RINEPT NMR spectra. The black and red lines correspond to the experimental and analytically simulated spectra, respectively. The exact parameters used to fit the ¹¹B spin echo spectra are given in Table S3. All spectra were recorded at $B_0 = 14.1$ T with 25 kHz MAS.

1D direct excitation ¹¹B spin echo NMR spectra of **S2**, **S7**, and **S9** display two main groups of signals centered at *ca*. 0 or 10 ppm, corresponding to 4-coordinate (BO₄) and three-coordinate (BO₃) boron oxide-type species, respectively (Figure 4, right column). ^{15, 21, 50-53} The broad signal

centered at ca. 10 ppm (BO₃-type species) can be analytically simulated to four unique boron sites with a C_0 between 2.2 and 2.5 MHz and $\delta_{iso}(^{11}\text{B}) \sim \text{(blue) } 17-19 \text{ ppm, (green) } 15 \text{ ppm, (orange)}$ 12 ppm, and (red) 10 ppm (Figure 4, right column, Table 1). The identification of each site is discussed below. We note that each ¹¹B fit in the analytical simulations have a significant amount of gaussian broadening to represent a distribution in shift/ C_Q caused by structural disorder, typical of surface supported boron oxide/hydroxide species. ¹⁵ 2D ¹¹B→¹H dipolar refocused INEPT (D-RINEPT) HETCOR spectra of S2, S7, and S9 recorded with a short duration of dipolar recoupling (0.96 ms) all display intense ¹H NMR signals at ca. 3 ppm correlating to ¹¹B NMR signals centered at ca. 12 - 14 ppm (Figure S8). The short duration of dipolar recoupling ensures that the ${}^{1}H$ and ¹¹B NMR signals arise from boron hydroxide species (B-OH); the ¹H NMR signal at *ca.* 3 ppm is assigned to B-OH, similar to that observed in B-MWW and B/SiO₂-IWI. 15, 17, 21 An analytical simulation of the 2D ¹¹B projections reveal that there are two unique boron species containing hydroxyl groups with $\delta_{iso}(^{11}B) \sim (green fit)$ 15 ppm or (blue fit) 17 – 19 ppm (Figure 4, right column). As the dipolar recoupling duration is increased to 2.9 ms, enabling the observation of H-B spin pairs further away in space, an additional correlation between the same ¹¹B NMR signals and a ¹H NMR signal at ca. 2 ppm is observed (Figure 4, left column). The ¹H NMR signal at ca. 2 ppm is assigned to a nearby isolated (i.e., not hydrogen bonded) silanol (Si-OH) group (Figure 5. S9).^{51, 57, 60}

The 2D 1 H- 11 B HETCOR spectra identified B-OH containing boron species and revealed that they are in close-spatial proximity to isolated silanol groups. It is well known that $\delta_{iso}({}^{11}$ B) decreases as B-O-**B** groups are replaced with B-O-**Si**; **B**(OB)₃ and **B**(OSi)₃ on silica/zeolites typically resonance at *ca*. 17 and 10 ppm, respectively. 15 , 50 - 51 , 61 - 64 Therefore, based on the high $\delta_{iso}({}^{11}$ B) and strong 1 H- 11 B HETCOR correlations observed with a short duration of recoupling,

we assign the ¹¹B NMR signals at $\delta_{iso}(^{11}B) \sim 17 - 19$ ppm to $\mathbf{B}(OB)_x(OH)_{3-x}$ (x = 1 - 2) exhibiting at least one B-O-B and B-O-H bond (Table 1). The ^{11}B NMR signal at $\delta_{iso}(^{11}B)\sim15$ ppm also displays strong ¹H-¹¹B heteronuclear correlations and thus contains a B-OH bond. However, the decrease in shift is likely a result of replacing a B-O-B group with B-O-Si, suggesting this species corresponds to $\mathbf{B}(OB)_x(OH)_{2-x}(OSi)$ (x = 0 - 1) (Table 1). The ¹¹B NMR signals at ~ 10 and 12 ppm observed in the direct excitation experiment were not observed in the ¹H-¹¹B HETCOR spectra and thus do not contain a hydroxyl group. Based on well-established literature and the low observed $\delta_{iso}(^{11}B)$, the ^{11}B NMR signals at $\delta_{iso}(^{11}B) \sim 12$ and 10 ppm correspond to $\mathbf{B}(OB)(OSi)_2$ and B(OSi)₃ species, respectively (Table 1). 15, 50-51, 61-64 1D 11B dipolar DO-SO NMR spectra of S2 and S7 resemble that of 1D direct excitation ¹¹B NMR spectra, corroborating our NMR assignments and illustrating that the majority of 3-coordinate boron is clustered on the silica surface (Figure S10). It should be noted that we were unsuccessful in recording a ¹¹B DQ-SQ spectrum of S9, however, this is attributed to low sensitivity associated with the DQ-SQ experiment and low B weight loading (~0.18 wt %) on the silica surface. Lastly, no 4-coordinate BO₄ species were observed in the ¹H-¹¹B HETOR spectra, revealing that BO₄ is not proximate to ¹H spins. The **B**O₄ species are likely charge balanced by ion impurities in the silica, such as Na⁺, ²⁴, 65 which has been previously reported for borosilicate zeolites. 51 Therefore, we hypothesize that **B**O₄ is likely incorporated into the silica framework, taking the formula **B**(OSi)₄ (Table 1).

Table 1. Structure of boron species, NMR parameters, and percent population for each $Bpin/SiO_{2(T)}$ -500v material.

Species ^a	B/H O B/O B/H	B/H O B/O B/H - O O O	0-Si-O -O, B'O, B'O	0-Si-0 0-Si-0 0-Si-0	0 B 0 Si-0
	$B(OB)(OB/H)_2$	B(OB/H) ₂ (OSi)	$B(OB)(OSi)_2$	B(OSi) ₃	B(OSi) ₄
δ_{iso} (ppm)	~17-19	~15	~12	~10	~0
C _Q (MHz)	2.4-2.5	2.2	2.2	2.3	0.5
	Percent Population (%)				
Bpin/SiO ₂₍₂₀₀₎ -500v	24	29	25	13	9
Bpin/SiO ₂₍₇₀₀₎ -500v	17	32	29	10	12
Bpin/SiO ₂₍₉₀₀₎ -500v	27	33	18	10	12

^aSpecies with "OB/H" means it is either an O-B or O-H functional group.

The analytical simulations of the 1D 11 B NMR spectra (recycle delay > 5 × T_1) suggest that the relative populations of each type of boron species is similar between all catalysts, with minor differences that are likely within error of the simulations (Table 1). However, comparison of 1 H NMR spectra reveal significant differences between the catalysts (Figure 5). A 1 H DQ-SQ NMR spectrum of S2 displays an intense, broad signal centered at ca. 4 ppm which is assigned to hydrogen-bonded Si-OH species (Figure 5 and S11). Alternatively, this broad NMR signal at 4 ppm is nearly absent in the 1 H DQ-SQ NMR spectrum of S7 and is completely absent in the 1 H DQ-SQ NMR spectrum of S9, revealing that the hydrogen bonding network in the active catalysts is significantly reduced with increased SiO₂ thermal pre-treatment temperatures (Figure 5 and S11). The observation of decreased hydrogen bonding with increased SiO₂ thermal treatment is

consistent with that observed in the transmission IR spectra discussed above (Figure S6). Closer inspection of the ¹¹B→¹H D-RINEPT NMR spectra of S2, S7, and S9 shows there are two unique B-OH ¹H chemical shifts at ca. 3.0 and 3.4 ppm. Interestingly, only the B-OH ¹H NMR signal at ca. 3.4 ppm is observed in the ¹H DQ-SQ spectra of S7 and S9 and displays autocorrelations, showing that the B-OH ¹H NMR signal at ca. 3.4 ppm is proximate to another B-OH species while the B-OH 1 H NMR signal at ca. 3.0 ppm is relatively isolated (within ~ 5 Å distance) from other hydrogen atoms (Figure S11). We note there are two additional ¹H NMR signals at ca. 0 and 1 ppm that come through the DQ-filter that did not reveal correlations to ¹¹B (Figure 4, 5, S8 and S11). The ¹H NMR signal at ca. 1 ppm has been previously assigned to water-inaccessible or internal non-hydrogen bonded Si-OH species that likely reside inside the silica rather than near or on the surface; 66-69 the Si-OH ¹H NMR signal at ca. 2 ppm is likely near or on the surface as it correlated to the surface boron oxide/hydroxide ¹¹B NMR signals (Figure 4, left column). Therefore, we assign the ¹H NMR signal at ca. 1 ppm to internal non-hydrogen bonded Si-OH species. The ¹H NMR signal at ca. 0 ppm is preliminarily assigned to silicone vacuum grease impurities that immobilized on the silica surface during the thermal treatment of Bpin/SiO_{2(T)}. We note that the 0 ppm ¹H NMR signal was also observed in the as-grafted materials, further suggesting assignment to silicone vacuum grease (Figure S5).

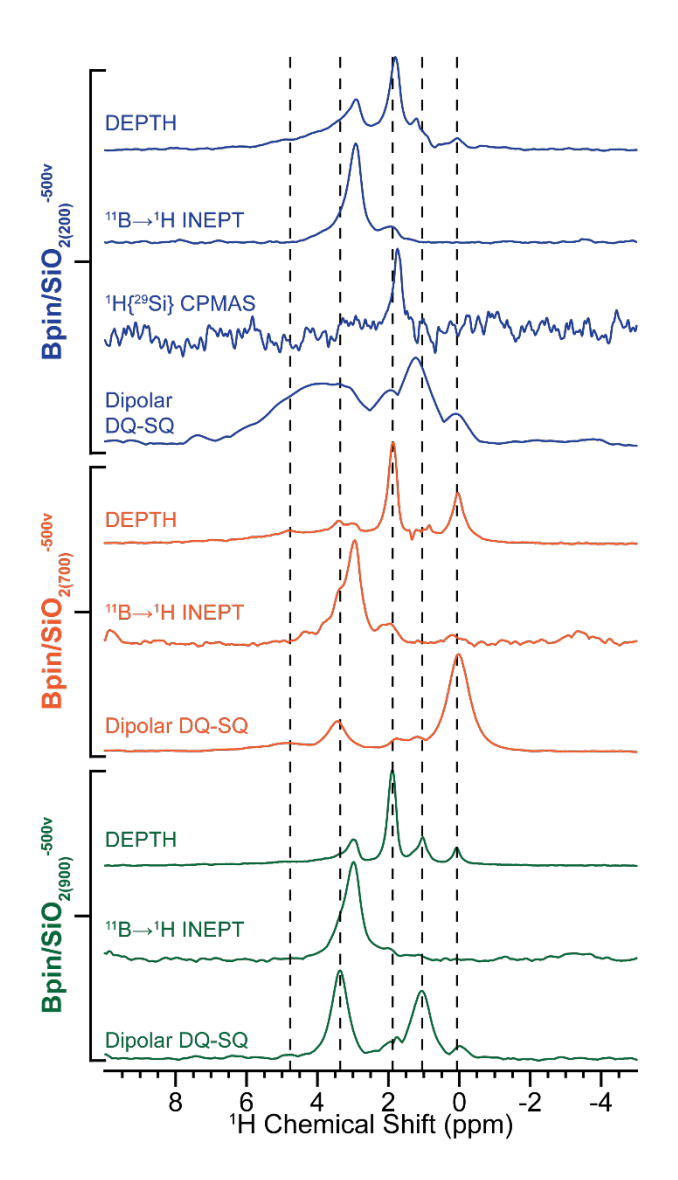


Figure 5. Comparison of 1D direct excitation (DEPTH) 1 H, 11 B \rightarrow 1 H D-RINEPT, 1 H $\{^{29}$ Si $\}$ CPMAS and 1 H DQ-SQ spectra for (upper, blue) Bpin/SiO₂₍₂₀₀₎- 500 v, (middle, orange) Bpin/SiO₂₍₇₀₀₎- 500 v and (lower, green) Bpin/SiO₂₍₉₀₀₎- 500 v. The exact experiment is given above each spectrum. All spectra were recorded at $B_0 = 14.1$ T with 25 kHz MAS.

In summary, ^{11}B solid-state NMR spectroscopy revealed that the boron speciation after thermal treatment is not dependent on the initial silanol density or the boron weight loading. The grafted materials, $Bpin/SiO_{2(T)}$, contained monopodally grafted molecular boron and the number of

neighboring hydrogen bonded silanol groups was controlled by the temperature of SiO₂ thermal pretreatment, where Bpin/SiO₂₍₉₀₀₎ exhibited little to no hydrogen-bonded silanol species. Therefore, the observation of similar boron species for all catalysts illustrates that boron oxide/hydroxide can move around on the surface of SiO₂ under the thermal treatment conditions to form an agglomerated boron oxide/hydroxide phase regardless of boron weight loading and surface hydrogen bonding networks. The boron speciation and the presence of a large proportion of silanol groups suggests the formation of small boron clusters or particles rather than an even monolayer on the support surface. ¹H solid-state NMR and FTIR spectroscopies suggest that the main difference between the different catalyst materials is the hydrogen bonding network on the surface of silica, where increased silica pretreatment temperatures lead to decreased surface hydrogen bonding networks, as expected. Future studies should evaluate the effect of thermal treatment conditions on the boron speciation.

3.3 Evaluating catalytic activity and changes in boron structure.

Propane ODH experiments were performed in a fixed bed quartz reactor at 500 °C under a mixture of C₃H₈, O₂, and N₂ in a 6:3:11 molar ratio. The conversion stabilized over 24 hours (Figure 6A), after which the gas flow rates were changed to acquire the conversion-selectivity trends shown in Figure 6B. As is seen in Figure 6A, each material undergoes an induction period before reaching steady-state conversion. For each catalyst, steady-state conversion is *ca.* 2 %

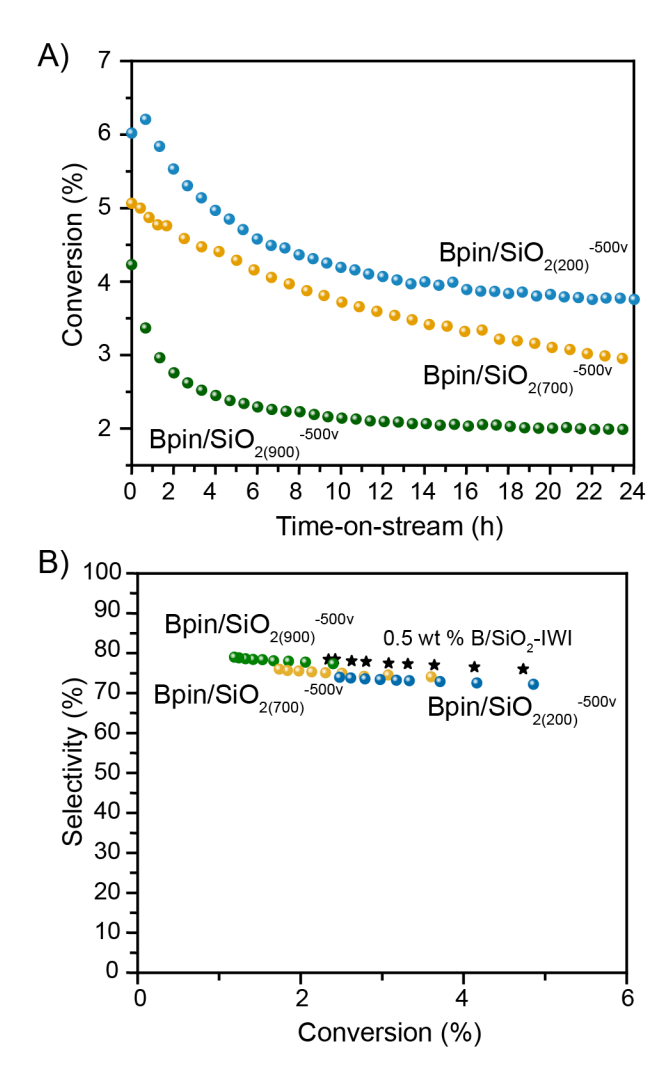


Figure 6. (A) Conversion as a function of time-on-stream and (B) Propylene selectivity as a function of propane conversion. Different conversions were achieved by changing the gas flow rate between 40 and 200 mL min⁻¹.

lower than the initial conversion. We presume that some boron is removed from the surface during this induction period as the surface likely restructures under reaction conditions. Elemental analysis of the catalysts after reaction showed that the boron weight loading of **S2** and **S7** decreased from 1.65 to 0.33 wt.% and 0.81 to 0.32 wt.%, respectively (Table S2). The weight loading of the spent **S9** sample could not be reliably determined, likely because of very low boron content (0.18 wt. % initial B loading). The conversion-selectivity trends in Figure 6B are typical of other B/SiO₂

catalysts in the literature. ^{16, 19, 21} There are slight differences in the conversion-selectivity trends between the materials which might be correlated with the amount of unselective silanol groups exposed on the surface.

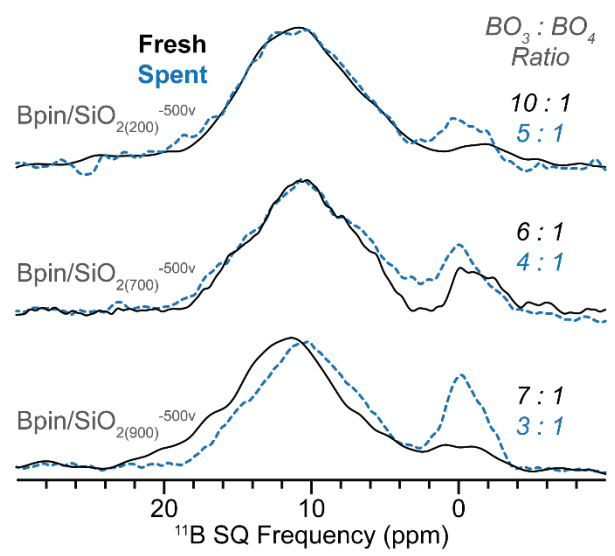


Figure 7. Comparison of relatively quantitative (recycle delay $\geq 5 \times T_1$) 1D ¹¹B spin echo NMR spectra of the B/spin/SiO_{2(T)}-500v materials (black, solid) before and (blue, dashed) after catalysis.

¹¹B solid-state NMR spectroscopy analysis of the catalysts after reaction do not show a drastic change in boron speciation (Figure 7). For each material, the ¹¹B NMR spectra for the spent catalysts (dashed blue lines) display similar 3-coordinate ¹¹B NMR signals as the fresh catalysts (solid black lines). Notably, there is an increase in the relative amount of BO₄ species in each sample. Based on the decrease in boron weight loading for **S2** and **S7** mentioned above, the relative increase in BO₄ is most likely due to leaching of surface BO₃ species; however, we cannot rule out the possibility of forming new **B**(OSi)₄ species under reaction conditions. There is also a clear loss of the boron-rich clusters that show up at the high frequency edge of the ¹¹B NMR spectrum of the **S9** material. This loss of boron-rich clusters is consistent with our previous observation that boroxol ring-type species are lost from B/SiO₂-IWI after catalysis. ^{15, 21} Notably, the shape of the

¹¹B NMR spectra for all spent catalysts are near identical, revealing that similar ODH active boron oxide/hydroxide clusters are present for all materials regardless of the initial silica thermal dehydration temperature (Figure S12). This further suggests that boron oxide/hydroxide is highly mobile on the silica surface under reaction conditions.

2D ¹¹B→¹H D-RINEPT spectra of the spent materials are also very similar to that of the fresh catalysts, with some minor differences in the ¹¹B projections likely due to the partial leaching of boron rich clusters containing hydroxyl groups (Figure S13 and S14). It should be mentioned that the 2D ¹¹B→¹H D-RINEPT spectra of the spent catalysts required significantly longer experimental times which is consistent with a decrease in boron loading after reaction and the partial removal of boron hydroxide species (Table S1). ¹⁵ Interestingly, ¹H dipolar DQ-SQ spectra of fresh S7 and S9 are significantly different than the spent materials (Figure S15). All spent catalysts reveal an intense, broad feature center at *ca.* 4-5 ppm in the ¹H DQ-SQ spectra which is assigned to hydrogen-bonded surface silanol species. This broad hydrogen-bonded surface silanol species was present in fresh S2 but was near absent in fresh S7 and completely absent in fresh S9 (Figure 5 and S15). The observation of surface hydrogen-bonding silanol species after catalysis for S7 and S9 further confirms the restructuring and partial leaching of boron oxide/hydroxide clusters under reaction conditions.

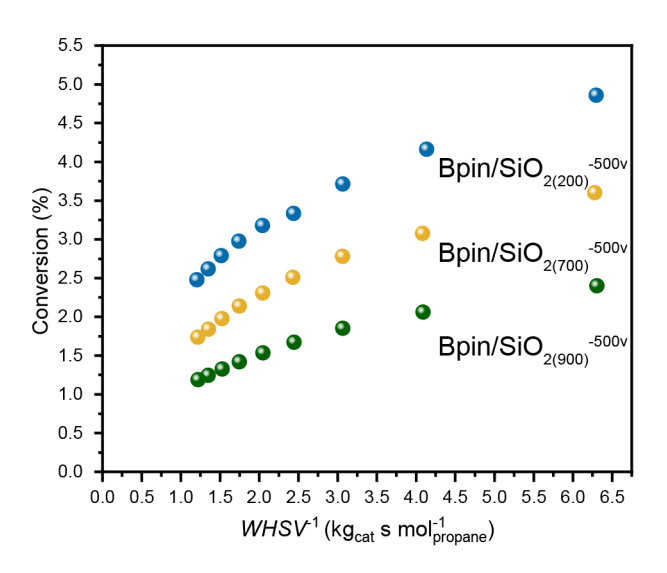


Figure 8. Propane conversion as a function of inverse weight hourly space velocity for all $Bpin/SiO_{2(T)}^{-500v}$ materials.

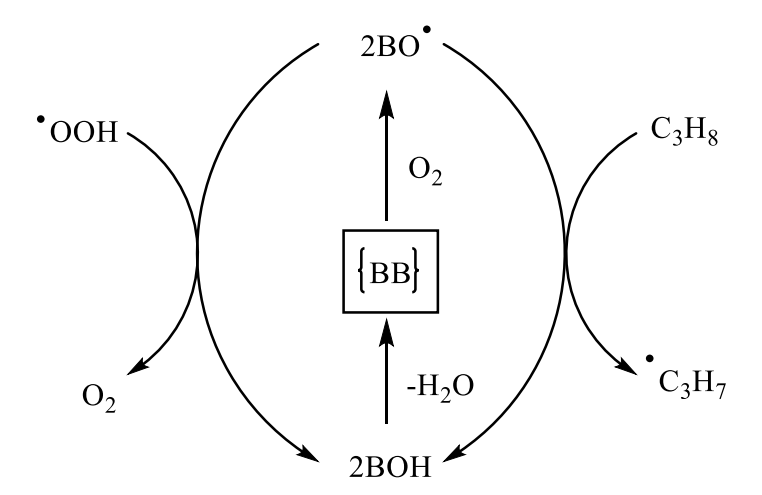
Although these materials do not allow us to probe the effect of initial boron agglomeration, we can probe the effect of boron weight loading on catalyst activity, uncomplicated by differences in initial boron speciation. We emphasize that we do not attempt to ascribe the catalytic activity to any one boron species. Rather, we seek to understand activity based on the overall structure and composition of the catalyst surface. Because the boron oxide/hydroxide phase is dynamic under reaction conditions, the accessible structures under such conditions are likely distinct from those observed at room temperature using *ex situ* characterization, where the most thermodynamically favorable phases are detected.

Figure 8 shows the propane conversion as a function of inverse weight-hourly-space-velocity (*i.e.*, the contact time between the gas and the surface) for each catalyst. As expected, when weight loading increases, the conversion at a given contact time increases. Often, such a plot is fit with a linear line to determine the initial reaction rate. However, for all three materials, the conversion begins to level off at higher contact times. This is unlike the behavior of the bulk boron-based

materials, which show a linear increase of conversion as the contact time increases.² This difference suggests that the observed catalytic results do not have a straightforward interpretation and are likely complicated by the gas phase chemistry that occurs during the reaction.

The propylene productivity normalized per mole of boron is shown in Figure S16. The S9 material is the most productive per mole B, followed by S7, then S2. This trend is consistent with the formation of different sized particles on the surface of the materials. The particles on S9 are smaller than those on the higher weight loading S2 material, so more boron atoms are at the surface of the particles on S9 and are able to participate in the reaction. For each material, the normalized productivity decreases as the conversion and contact time increase. To understand this behavior, we must put these results into context with our hypothesized mechanism and the role the surface plays within that mechanism.

Scheme 1. Simplified proposed reaction network showing only reactions involving BO•. The square denotes the active site.



The proposed mechanism proceeds via a radical pathway.^{9-10, 18} The main role of the surface is to initiate the reaction by generating radical species.⁹ Under reaction conditions, the surface generates unsaturated {BB} units that can activate O₂ to form 2BO• species. As can be seen in the

simplified reaction network in Scheme 1, any reaction with BO• is a termination reaction that generates B-OH groups. B-OH groups are not readily reactive and must be dehydrated to regenerate active {BB} sites. The calculated barrier for this regeneration step is 222 kJ/mol, ¹⁰ in line with experimentally reported apparent activation energies of 200-250 kJ/mol for hBN-catalyzed ODH.^{3, 10} Based on the closeness of the calculated barrier and experimental activation energies, we have hypothesized that active site regeneration is the rate-limiting reaction step in the overall mechanism. We emphasize that the hypothesized BO• surface species would only form under reaction conditions and that such a species would not be detected using *ex situ* characterization techniques.

While more systematic kinetic studies are needed to better understand the behavior of these supported materials, the proposed mechanism offers a possible explanation for the observed loss of activity at higher conversions. As the gas moves more slowly through the catalyst bed, more active sites are consumed. The consumption of the active sites leads to the eventual formation of unreactive B-OH groups that must be regenerated. If active site regeneration is indeed rate limiting, perhaps the loss of productivity per mole B occurs because at high conversions, the reaction becomes limited, as there is a fixed amount of boron available in a given cluster or particle on SiO₂, and the surface can eventually become saturated in B-OH groups, decreasing the active site concentration and the rate of initiation. Such saturation-like behavior does not occur with bulk materials where boron is abundant. A more thorough exploration of the reaction kinetics over these materials is ongoing in our lab.

4. Conclusions

A combination of transmission FTIR and solid-state NMR spectroscopies revealed that the grafting of HBpin onto SiO_2 generates isolated, monopodally grafted Bpin (B-O-Si bond to the silica surface) that can form hydrogen bonds with nearby unreacted silanol groups. The number of neighboring hydrogen-bonded silanol species can be decreased with increased silica thermal treatment temperature, enabling high controllability of the local chemical environment surrounding the isolated, singly anchored Bpin molecule. However, the control over surface speciation is lost during the thermal treatment of Bpin/SiO_{2(T)} materials, as a similar boron oxide/hydroxide phase is observed for all catalysts. The observation of similar boron species, especially for **S9**, which contained ~ 0.18 wt. % B and exhibited highly isolated grafted Bpin before thermal treatment, illustrates that boron oxide/hydroxide is highly mobile on the SiO₂ surface and is able to generate clustered boron oxide/hydroxide under thermal treatment conditions. Modification of thermal treatment conditions, chemically treating the surface before or after grafting, and/or doping the silica surface could potentially enable better control over the species formed on the silica surface by reducing boron oxide/hydroxide mobility.

The catalytic activity of Bpin/SiO_{2(T)}-500v materials is typical for silica-supported boron oxide catalysts previously reported.^{19, 21} Because these materials of different boron weight loadings contained similar boron speciation, we were able to probe the effect of boron content on catalytic activity. We observed the highest propylene productivity per mole of boron in the **S9** material, consistent with the presence of boron oxide/hydroxide particles. Additionally, we observed the loss of productivity at increased conversions for all catalysts. More thorough kinetic studies are needed to understand this observation in terms of the proposed reaction mechanism.

Supporting Information

Additional FTIR and solid-state NMR spectra, catalytic data, and solid-state NMR experimental parameters table.

Author Information

Corresponding Authors

Aaron J. Rossini – Department of Chemistry, Iowa State University, Ames, Iowa 50011, United States; Ames Laboratory, US Department of Energy, Ames, Iowa 50011, United States; http://orcid.org/0000-0002-1679-9203; Email: arossini@iastate.edu

Ive Hermans - Department of Chemistry, University of Wisconsin – Madison, Madison, Wisconsin 53706, United States; Department of Chemical and Biological Engineering, University of Wisconsin – Madison, Madison, Wisconsin 53706, United States; http://orcid.org/0000-0001-6228-9928; Email: hermans@chem.wisc.edu

Present Addresses

Melissa C. Cendejas - Department of Chemistry, University of Wisconsin – Madison, Madison, Wisconsin 53706, United States

Rick W. Dorn - Department of Chemistry, Iowa State University, Ames, Iowa 50011, United States; Ames Laboratory, US Department of Energy, Ames, Iowa 50011, United States

William P. McDermott - Department of Chemistry, University of Wisconsin - Madison, Madison, Wisconsin 53706, United States

Edgard A. Lebrón-Rodríguez - Department of Chemical and Biological Engineering,

University of Wisconsin - Madison, Madison, Wisconsin 53706, United States

Lesli O. Mark - Department of Chemistry, University of Wisconsin – Madison, Madison, Wisconsin 53706, United States

Author Contributions

‡These authors contributed equally.

Acknowledgements This work was supported by the National Science Foundation under Grant No. CBET-1916809. AJR acknowledges additional support from the Alfred P. Sloan Foundation through a Sloan research fellowship. NMR Experiments performed at UW-Madison were supported by a generous gift from Paul J. and Margaret M. Bender and the UW2020 fund.

References

- (1) Grant, J. T.; Carrero, C. A.; Goeltl, F.; Venegas, J.; Mueller, P.; Burt, S. P.; Specht, S. E.; McDermott, W. P.; Chieregato, A.; Hermans, I., Selective Oxidative Dehydrogenation of Propane to Propene Using Boron Nitride Catalysts. *Science* **2016**, *354* (6319), 1570-1573. 10.1126/science.aaf7885.
- (2) Grant, J. T.; McDermott, W. P.; Venegas, J. M.; Burt, S. P.; Micka, J.; Phivilay, S. P.; Carrero, C. A.; Hermans, I., Boron and Boron-Containing Catalysts for the Oxidative Dehydrogenation of Propane. *ChemCatChem* **2017**, *9* (19), 3623-3626. 10.1002/cctc.201701140.
- (3) Venegas, J. M.; Grant, J. T.; McDermott, W. P.; Burt, S. P.; Micka, J.; Carrero, C. A.; Hermans, I., Selective Oxidation of N-Butane and Isobutane Catalyzed by Boron Nitride. *ChemCatChem* **2017**, *9* (12), 2118-2127. 10.1002/cctc.201601686.

- (4) Huang, R.; Zhang, B.; Wang, J.; Wu, K.-H.; Shi, W.; Zhang, Y.; Liu, Y.; Zheng, A.; Schlögl, R.; Su, D. S., Direct Insight into Ethane Oxidative Dehydrogenation over Boron Nitrides. *ChemCatChem* **2017**, *9* (17), 3293-3297. doi:10.1002/cctc.201700725.
- (5) Lei Shi, B. Y., Dan Shao, Fan Jiang, Dongqi Wang, An-Hui Lu, Selective Oxidative Dehydrogenation of Ethane to Ethylene over a Hydroxylated Boron Nitride Catalyst. *Chinese J Catal* **2017**, *38* (2), 389-395. 10.1016/s1872-2067(17)62786-4.
- (6) Shi, L.; Wang, D.; Song, W.; Shao, D.; Zhang, W.-P.; Lu, A.-H., Edge-Hydroxylated Boron Nitride for Oxidative Dehydrogenation of Propane to Propylene. *ChemCatChem* **2017**, 9 (10), 1788-1793. doi:10.1002/cctc.201700004.
- (7) Cavani, F.; Ballarini, N.; Cericola, A., Oxidative Dehydrogenation of Ethane and Propane: How Far from Commercial Implementation? *Catal. Today* **2007**, *127* (1), 113-131. https://doi.org/10.1016/j.cattod.2007.05.009.
- (8) Ren, T.; Patel, M.; Blok, K., Olefins from Conventional and Heavy Feedstocks: Energy Use in Steam Cracking and Alternative Processes. *Energy* **2006**, *31* (4), 425-451. https://doi.org/10.1016/j.energy.2005.04.001.
- (9) Zhang, X.; You, R.; Wei, Z.; Jiang, X.; Yang, J.; Pan, Y.; Wu, P.; Jia, Q.; Bao, Z.; Bai, L., et al., Radical Chemistry and Reaction Mechanisms of Propane Oxidative Dehydrogenation over Hexagonal Boron Nitride Catalysts. *Angew. Chem.*, *Int. Ed.* **2020**, *59* (21), 8042-8046. 10.1002/anie.202002440.

- (10) Venegas, J. M.; Zhang, Z.; Agbi, T. O.; McDermott, W. P.; Alexandrova, A.; Hermans, I., Why Boron Nitride Is Such a Selective Catalyst for the Oxidative Dehydrogenation of Propane. *Angew. Chem. Int.l Ed.* **2020**, *59* (38), 16527-16535. 10.1002/anie.202003695.
- (11) Si, C.; Lian, Z.; Olanrele, S. O.; Sun, X.; Li, B., Revealing the Origin of the Reactivity of Metal-Free Boron Nitride Catalysts in Oxidative Dehydrogenation of Propane. *Appl. Surf. Sci.* **2020**, *519*, 146241. https://doi.org/10.1016/j.apsusc.2020.146241.
- (12) Rajbanshi, B.; Saha, S.; Fricke, C.; Ammal, S. C.; Heyden, A., Oxidative Dehydrogenation of Propane on the Oxygen Adsorbed Edges of Boron Nitride Nanoribbons. *Cat. Sci. Tech.* **2020**, *10* (15), 5181-5195. 10.1039/D0CY01031F.
- (13) Qiu, B.; Jiang, F.; Lu, W.-D.; Yan, B.; Li, W.-C.; Zhao, Z.-C.; Lu, A.-H., Oxidative Dehydrogenation of Propane Using Layered Borosilicate Zeolite as the Active and Selective Catalyst. *J. Catal.* **2020**, *385*, 176-182. https://doi.org/10.1016/j.jcat.2020.03.021.
- (14) McDermott, W. P.; Venegas, J.; Hermans, I., Selective Oxidative Cracking of N-Butane to Light Olefins over Hexagonal Boron Nitride with Limited Formation of Cox. *ChemSusChem* **2020**, *13* (1), 152-158. 10.1002/cssc.201901663.
- (15) Dorn, R. W.; Cendejas, M. C.; Chen, K.; Hung, I.; Altvater, N. R.; McDermott, W. P.; Gan, Z.; Hermans, I.; Rossini, A. J., Structure Determination of Boron-Based Oxidative Dehydrogenation Heterogeneous Catalysts with Ultrahigh Field 35.2 T 11b Solid-State Nmr Spectroscopy. *ACS Catal.* **2020**, *10* (23), 13852-13866. 10.1021/acscatal.0c03762.
- (16) Belgamwar, R.; Rankin, A. G. M.; Maity, A.; Mishra, A. K.; Gomez, J. S.; Trebosc, J.; Vinod, C. P.; Lafon, O.; Polshettiwar, V., Boron Nitride and Oxide Supported on Dendritic Fibrous

Nanosilica for Catalytic Oxidative Dehydrogenation of Propane. *ACS Sus. Chem. Eng.* **2020,** 8 (43), 16124-16135. 10.1021/acssuschemeng.0c04148.

- (17) Altvater, N. R.; Dorn, R. W.; Cendejas, M. C.; McDermott, W. P.; Thomas, B.; Rossini,
 A. J.; Hermans, I., B-Mww Zeolite: The Case against Single-Site Catalysis. *Angew. Chem. Int. Ed.*2020, 59 (16), 6546-6550. 10.1002/anie.201914696.
- (18) Venegas, J. M.; Hermans, I., The Influence of Reactor Parameters on the Boron Nitride-Catalyzed Oxidative Dehydrogenation of Propane. *Org. Process Res. & Dev.* **2018**, 22 (12), 1644-1652. 10.1021/acs.oprd.8b00301.
- (19) Lu, W.-D.; Wang, D.; Zhao, Z.; Song, W.; Li, W.-C.; Lu, A.-H., Supported Boron Oxide Catalysts for Selective and Low-Temperature Oxidative Dehydrogenation of Propane. *ACS Catal*. **2019**, *9* (9), 8263-8270. 10.1021/acscatal.9b02284.
- (20) Love, A. M.; Thomas, B.; Specht, S. E.; Hanrahan, M. P.; Venegas, J. M.; Burt, S. P.; Grant, J. T.; Cendejas, M. C.; McDermott, W. P.; Rossini, A. J., et al., Probing the Transformation of Boron Nitride Catalysts under Oxidative Dehydrogenation Conditions. *J. Am. Chem. Soc.* **2019**, *141* (1), 182-190. 10.1021/jacs.8b08165.
- (21) Love, A. M.; Cendejas, M. C.; Thomas, B.; McDermott, W. P.; Uchupalanun, P.; Kruszynski, C.; Burt, S. P.; Agbi, T.; Rossini, A. J.; Hermans, I., Synthesis and Characterization of Silica-Supported Boron Oxide Catalysts for the Oxidative Dehydrogenation of Propane. *J. Phys. Chem. C* **2019**, *123* (44), 27000-27011. 10.1021/acs.jpcc.9b07429.

- (22) Zhang, Z.; Jimenez-Izal, E.; Hermans, I.; Alexandrova, A. N., Dynamic Phase Diagram of Catalytic Surface of Hexagonal Boron Nitride under Conditions of Oxidative Dehydrogenation of Propane. *J. Phys. Chem. Let.* **2019**, *10* (1), 20-25. 10.1021/acs.jpclett.8b03373.
- (23) Carrero, C. A.; Burt, S. P.; Huang, F.; Venegas, J. M.; Love, A. M.; Mueller, P.; Zhu, H.; Grant, J. T.; Mathison, R.; Hanraham, M. P., et al., Supported Two- and Three-Dimensional Vanadium Oxide Species on the Surface of B-Sic. *Cat. Sci. Tech.* **2017**, *7* (17), 3707-3714. 10.1039/C7CY01036B.
- (24) Grant, J. T.; Carrero, C. A.; Love, A. M.; Verel, R.; Hermans, I., Enhanced Two-Dimensional Dispersion of Group V Metal Oxides on Silica. *ACS Catal.* **2015**, *5* (10), 5787-5793. 10.1021/acscatal.5b01679.
- (25) Williams, L. A.; Marks, T. J., Synthesis, Characterization, and Heterogeneous Catalytic Implementation of Sulfated Alumina Nanoparticles. Arene Hydrogenation and Olefin Polymerization Properties of Supported Organozirconium Complexes. *ACS Catal.* **2011**, *1* (4), 238-245. 10.1021/cs100119w.
- (26) Chabanas, M.; Vidal, V.; Copéret, C.; Thivolle-Cazat, J.; Basset, J.-M., Low-Temperature Hydrogenolysis of Alkanes Catalyzed by a Silica-Supported Tantalum Hydride Complex, and Evidence for a Mechanistic Switch from Group Iv to Group V Metal Surface Hydride Complexes. *Angew. Chem. Int. Ed.* **2000,** *39* (11), 1962-1965. <a href="https://doi.org/10.1002/1521-3773(20000602)39:11<1962::AID-ANIE1962>3.0.CO;2-1.">https://doi.org/10.1002/1521-3773(20000602)39:11<1962::AID-ANIE1962>3.0.CO;2-1.
- (27) Love, A. M.; Cendejas, M. C.; Hanrahan, M. P.; Carnahan, S. L.; Uchupalanun, P.; Rossini, A. J.; Hermans, I., Understanding the Synthesis of Supported Vanadium Oxide Catalysts Using Chemical Grafting. *Chem.Eur. J.* **2020**, *26* (5), 1052-1063. 10.1002/chem.201904260.

- (28) Love, A. M.; Carrero, C. A.; Chieregato, A.; Grant, J. T.; Conrad, S.; Verel, R.; Hermans, I., Elucidation of Anchoring and Restructuring Steps During Synthesis of Silica-Supported Vanadium Oxide Catalysts. *Chem. Mater.* **2016,** 28 (15), 5495-5504. 10.1021/acs.chemmater.6b02118.
- (29) Copéret, C., Single-Sites and Nanoparticles at Tailored Interfaces Prepared Via Surface Organometallic Chemistry from Thermolytic Molecular Precursors. *Acc. Chem. Res.* **2019**, *52* (6), 1697-1708. 10.1021/acs.accounts.9b00138.
- (30) Fujdala, K. L.; Brutchey, R. L.; Tilley, T. D., Tailored Oxide Materials Via Thermolytic Molecular Precursor (Tmp) Methods. In *Surface and Interfacial Organometallic Chemistry and Catalysis*, Copéret, C.; Chaudret, B., Eds. Springer Berlin Heidelberg: Berlin, Heidelberg, **2005**; pp 69-115.
- (31) Harris, R. K.; Becker, E. D.; Cabral de Menezes, S. M.; Goodfellow, R.; Granger, P., Nmr Nomenclature: Nuclear Spin Properties and Conventions for Chemical Shifts: Iupac Recommendations 2001. *Solid State Nuc. Magn. Res.* **2002,** 22 (4), 458-483. https://doi.org/10.1006/snmr.2002.0063.
- (32) Mali, G.; Fink, G.; Taulelle, F., Double-Quantum Homonuclear Correlation Magic Angle Sample Spinning Nuclear Magnetic Resonance Spectroscopy of Dipolar-Coupled Quadrupolar Nuclei. *J. Chem. Phys.* **2004**, *120* (6), 2835-2845. 10.1063/1.1638741.
- (33) Edén, M.; Zhou, D.; Yu, J., Improved Double-Quantum Nmr Correlation Spectroscopy of Dipolar-Coupled Quadrupolar Spins. *Chem. Phys. Lett.* **2006**, *431* (4), 397-403. https://doi.org/10.1016/j.cplett.2006.09.081.

- (34) Yao, Z.; Kwak, H.-T.; Sakellariou, D.; Emsley, L.; Grandinetti, P. J., Sensitivity Enhancement of the Central Transition Nmr Signal of Quadrupolar Nuclei under Magic-Angle Spinning. *Chem. Phys. Lett.* **2000**, *327* (1), 85-90. https://doi.org/10.1016/S0009-2614(00)00805-8.
- (35) Kwak, H.-T.; Prasad, S.; Clark, T.; Grandinetti, P. J., Enhancing Sensitivity of Quadrupolar Nuclei in Solid-State Nmr with Multiple Rotor Assisted Population Transfers. *Solid State Nuc. Magn. Res.* **2003**, *24* (2), 71-77. https://doi.org/10.1016/S0926-2040(03)00051-1.
- (36) Wang, Q.; Li, Y.; Trébosc, J.; Lafon, O.; Xu, J.; Hu, B.; Feng, N.; Chen, Q.; Amoureux, J.-P.; Deng, F., Population Transfer Hmqc for Half-Integer Quadrupolar Nuclei. *J. Chem. Phys.* **2015**, *142* (9), 094201. 10.1063/1.4913683.
- (37) Fung, B. M.; Khitrin, A. K.; Ermolaev, K., An Improved Broadband Decoupling Sequence for Liquid Crystals and Solids. *J. Magn.*. *Reson.* **2000,** *142* (1), 97-101. https://doi.org/10.1006/jmre.1999.1896.
- (38) Feike, M.; Demco, D. E.; Graf, R.; Gottwald, J.; Hafner, S.; Spiess, H. W., Broadband Multiple-Quantum Nmr Spectroscopy. *J Magn. Reson. A* **1996,** *122* (2), 214-221. https://doi.org/10.1006/jmra.1996.0197.
- (39) Schnell, I.; Lupulescu, A.; Hafner, S.; Demco, D. E.; Spiess, H. W., Resolution Enhancement in Multiple-Quantum Mas Nmr Spectroscopy. *J. Magn. Reson.* **1998**, *133* (1), 61-69. https://doi.org/10.1006/jmre.1998.1432.

- (40) Trebosc, J.; Hu, B.; Amoureux, J. P.; Gan, Z., Through-Space R3-Hetcor Experiments between Spin-1/2 and Half-Integer Quadrupolar Nuclei in Solid-State Nmr. *J. Magn. Reson.* **2007**, 186 (2), 220-227. https://doi.org/10.1016/j.jmr.2007.02.015.
- (41) Venkatesh, A.; Hanrahan, M. P.; Rossini, A. J., Proton Detection of Mas Solid-State Nmr Spectra of Half-Integer Quadrupolar Nuclei. *Solid State Nuc. Magn. Res.* **2017**, 84, 171-181. https://doi.org/10.1016/j.ssnmr.2017.03.005.
- (42) Venkatesh, A.; Luan, X.; Perras, F. A.; Hung, I.; Huang, W.; Rossini, A. J., T 1-Noise Eliminated Dipolar Heteronuclear Multiple-Quantum Coherence Solid-State Nmr Spectroscopy. *Phys. Chem. Chem. Phys.* **2020**, 22 (36), 20815-20828. 10.1039/D0CP03511D.
- (43) Brinkmann, A.; Kentgens, A. P. M., Proton-Selective 17o–H Distance Measurements in Fast Magic-Angle-Spinning Solid-State Nmr Spectroscopy for the Determination of Hydrogen Bond Lengths. *J. Am. Chem. Soc.* **2006**, *128* (46), 14758-14759. 10.1021/ja065415k.
- (44) Venkatesh, A.; Ryan, M. J.; Biswas, A.; Boteju, K. C.; Sadow, A. D.; Rossini, A. J., Enhancing the Sensitivity of Solid-State Nmr Experiments with Very Low Gyromagnetic Ratio Nuclei with Fast Magic Angle Spinning and Proton Detection. *J. Phys. Chem. A* **2018**, *122* (25), 5635-5643. 10.1021/acs.jpca.8b05107.
- (45) Ishii, Y.; Tycko, R., Sensitivity Enhancement in Solid State 15n Nmr by Indirect Detection with High-Speed Magic Angle Spinning. *J. Magn. Reson.* **2000,** *142* (1), 199-204. https://doi.org/10.1006/jmre.1999.1976.
- (46) Mathey, L.; Alphazan, T.; Valla, M.; Veyre, L.; Fontaine, H.; Enyedi, V.; Yckache, K.; Danielou, M.; Kerdiles, S.; Guerrero, J., et al., Functionalization of Silica Nanoparticles and Native

Silicon Oxide with Tailored Boron-Molecular Precursors for Efficient and Predictive P-Doping of Silicon. *J. Phys. Chem. C* **2015**, *119* (24), 13750-13757. 10.1021/acs.jpcc.5b03408.

- (47) Agarwala, A.; Subramani, T.; Goldbourt, A.; Danovich, D.; Yerushalmi, R., Facile Monolayer Formation on Sio2 Surfaces Via Organoboron Functionalities. *Angew. Chem. Int. Ed.* **2013**, *52* (29), 7415-7418. 10.1002/anie.201302655.
- (48) Rascón, F.; Wischert, R.; Copéret, C., Molecular Nature of Support Effects in Single-Site Heterogeneous Catalysts: Silicavs. Alumina. *Chem. Sci.* **2011,** 2 (8), 1449-1456. 10.1039/C1SC00073J.
- (49) Zhuravlev, L. T., The Surface Chemistry of Amorphous Silica. Zhuravlev Model. *Colloids Surf. A. Physicochem. Eng. Asp.* **2000,** *173* (1), 1-38. https://doi.org/10.1016/S0927-7757(00)00556-2.
- (50) Angel Wong, Y.-T.; Bryce, D. L., Chapter Four Recent Advances in 11b Solid-State Nuclear Magnetic Resonance Spectroscopy of Crystalline Solids. In *Annual Reports on Nmr Spectroscopy*, Webb, G. A., Ed. Academic Press: 2018; Vol. 93, pp 213-279.
- (51) Hwang, S.-J.; Chen, C.-Y.; Zones, S. I., Boron Sites in Borosilicate Zeolites at Various Stages of Hydration Studied by Solid State Nmr Spectroscopy. *J. Phys. Chem. B* **2004**, *108* (48), 18535-18546. 10.1021/jp0476904.
- (52) Kroeker, S.; Stebbins, J. F., Three-Coordinated Boron-11 Chemical Shifts in Borates. *Inorg. Chem.* **2001**, *40* (24), 6239-6246. 10.1021/ic010305u.
- (53) Hwang, S. J.; Fernandez, C.; Amoureux, J. P.; Cho, J.; Martin, S. W.; Pruski, M., Quantitative Study of the Short Range Order in B2o3 and B2s3 by Mas and Two-Dimensional

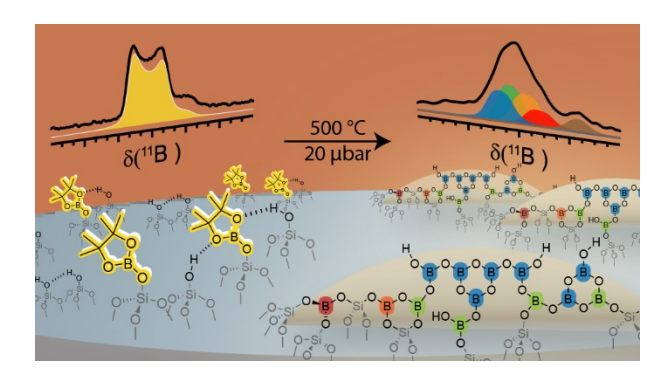
- Triple-Quantum Mas 11b Nmr. *Solid State Nuc. Magn. Res.* **1997,** 8 (2), 109-121. https://doi.org/10.1016/S0926-2040(96)01280-5.
- (54) Kong, X.; O'Dell, L. A.; Terskikh, V.; Ye, E.; Wang, R.; Wu, G., Variable-Temperature 170 Nmr Studies Allow Quantitative Evaluation of Molecular Dynamics in Organic Solids. *J.Am. Chem. Soc.* **2012**, *134* (35), 14609-14617. 10.1021/ja306227p.
- (55) Dračínský, M.; Hodgkinson, P., A Molecular Dynamics Study of the Effects of Fast Molecular Motions on Solid-State Nmr Parameters. *CrystEngComm* **2013**, *15* (43), 8705-8712. 10.1039/C3CE40612A.
- (56) Eedugurala, N.; Wang, Z.; Chaudhary, U.; Nelson, N.; Kandel, K.; Kobayashi, T.; Slowing, I. I.; Pruski, M.; Sadow, A. D., Mesoporous Silica-Supported Amidozirconium-Catalyzed Carbonyl Hydroboration. *ACS Catal.* **2015**, *5* (12), 7399-7414. 10.1021/acscatal.5b01671.
- (57) Trébosc, J.; Wiench, J. W.; Huh, S.; Lin, V. S. Y.; Pruski, M., Solid-State Nmr Study of Mcm-41-Type Mesoporous Silica Nanoparticles. *J. Am. Chem. Soc.* **2005**, *127* (9), 3057-3068. 10.1021/ja043567e.
- (58) Andrews, L.; Burkholder, T. R., Infrared Spectra of Molecular B(OH)3 and Hobo in Solid Argon. *J. Chem. Phys.* **1992,** 97 (10), 7203-7210. 10.1063/1.463545.
- (59) Gilson, T. R., Characterisation of Ortho- and Meta-Boric Acids in the Vapour Phase. *J. Chem. Soc.*, *Dalton Trans.* **1991**, (9), 2463-2466. 10.1039/DT9910002463.
- (60) Chen, J.; Liang, T.; Li, J.; Wang, S.; Qin, Z.; Wang, P.; Huang, L.; Fan, W.; Wang, J., Regulation of Framework Aluminum Siting and Acid Distribution in H-Mcm-22 by Boron

Incorporation and Its Effect on the Catalytic Performance in Methanol to Hydrocarbons. *ACS Catal.* **2016**, *6* (4), 2299-2313. 10.1021/acscatal.5b02862.

- (61) Koller, H.; Fild, C.; Lobo, R. F., Variable Anchoring of Boron in Zeolite Beta. *Microporous and Mesoporous Mater.* **2005,** 79 (1), 215-224. https://doi.org/10.1016/j.micromeso.2004.10.035.
- (62) Lezcano-González, I.; Vidal-Moya, A.; Boronat, M.; Blasco, T.; Corma, A., Modelling Active Sites for the Beckmann Rearrangement Reaction in Boron-Containing Zeolites and Their Interaction with Probe Molecules. *Phys. Chem. Chem. Phys.* **2010**, *12* (24), 6396-6403. 10.1039/C002427A.
- (63) Tong, H. T. T.; Koller, H., Control of Al for B Framework Substitution in Zeolite Beta by Counterions. *Microporous and Mesoporous Mater*. **2012,** *148* (1), 80-87. https://doi.org/10.1016/j.micromeso.2011.07.021.
- (64) Wiper, P. V.; Amelse, J.; Mafra, L., Multinuclear Solid-State Nmr Characterization of the Brønsted/Lewis Acid Properties in the Bp Hams-1b (H-[B]-Zsm-5) Borosilicate Molecular Sieve Using Adsorbed Tmpo and Tbpo Probe Molecules. *J. Catal.* **2014**, *316*, 240-250. https://doi.org/10.1016/j.jcat.2014.05.017.
- (65) Grant, J. T.; Love, A. M.; Carrero, C. A.; Huang, F.; Panger, J.; Verel, R.; Hermans, I., Improved Supported Metal Oxides for the Oxidative Dehydrogenation of Propane. *Top. Catal.* **2016**, *59* (17), 1545-1553. 10.1007/s11244-016-0671-2.

- (66) Hartmeyer, G.; Marichal, C.; Lebeau, B.; Rigolet, S.; Caullet, P.; Hernandez, J., Speciation of Silanol Groups in Precipitated Silica Nanoparticles by 1h Mas Nmr Spectroscopy. *J. Phys. Chem. C* **2007**, *111* (26), 9066-9071. 10.1021/jp0714901.
- (67) Dorémieux-Morin, C.; Heeribout, L.; Dumousseaux, C.; Fraissard, J.; Hommel, H.; Legrand, A. P., Study of the Constitutive Superficial Water of Precipitated Amorphous Silicas Using 1h Nmr: Broad-Line at 4 K and Hr Mas at 300 K. *J. Am. Chem. Soc.* **1996**, *118* (51), 13040-13045. 10.1021/ja962057k.
- (68) Kim, H. N.; Lee, S. K., Atomic Structure and Dehydration Mechanism of Amorphous Silica: Insights from 29si and 1h Solid-State Mas Nmr Study of Sio2 Nanoparticles. *Geochimica et Cosmochimica Acta* **2013**, *120*, 39-64. https://doi.org/10.1016/j.gca.2013.05.047.
- (69) Paris, M.; Fritsch, E.; Aguilar Reyes, B. O., 1h, 29si and 27al Nmr Study of the Destabilization Process of a Paracrystalline Opal from Mexico. *J. Non-Crystalline Solids* **2007**, 353 (16), 1650-1656. https://doi.org/10.1016/j.jnoncrysol.2006.12.111.

TOC



The image depicts the change in surface structure after the as-grafted material (left) is thermally treated to form the active catalyst material (right). The colors of the boron atoms correspond to the ¹¹B NMR analytical simulations.